CrossMark

Low-temperature molar heat capacity and thermodynamic properties of rare earth complex

[EuCu$_6$(µ-OH)$_3$(Gly)$_6$Im$_6$](ClO$_4$)$_6$·3H$_2$O
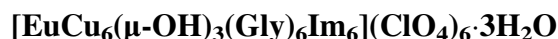
Lu Pan[1] · Xiao-Han Gao[1] · Xue-Chuan Lv[1] · Zhi-Cheng Tan[2]

Abstract A heptanuclear trigonal prismatic polyhedron, [EuCu$_6$(µ-OH)$_3$(Gly)$_6$Im$_6$](ClO$_4$)$_6$·3H$_2$O, was synthesized and characterized by elemental analysis and X-ray single-crystal diffraction. The complex crystallize is the rhombohedral R3 space group ($a = b = 15.8673$ Å, $c = 23.4038$ Å, $V = 5103.0(6)$ Å^3, $Z = 3$). In the clusters, Eu^{3+} ions are situated in the center of a prism formed by six copper atoms and coordinate to nine oxygen atoms with a tricapped trigonal prismatic coordination polyhedron. Six glycinato ligands and six imidazole terminal ligands (each coordinates to one Cu^{2+}) were used in the construction of the cluster. The low-temperature molar heat capacity, $C_{p,m}$, and thermodynamic properties of the complex were studied with an adiabatic calorimeter from 80 to 370 K. The thermodynamic functions [$H_T - H_{298.15}$] and [$S_T - S_{298.15}$] were derived in the temperature range from 80 to 370 K with a temperature interval of 5 K. The thermal properties of the complex from 300 to 800 K were studied by DSC and TG in nitrogen atmosphere.

Keywords Rare earth · Complex · Structure · Adiabatic calorimetry · Molar heat capacity

✉ Xue-Chuan Lv
  xuechuanster@163.com

  Zhi-Cheng Tan
  tzc@dicp.ac.cn

[1] School of Chemistry and Material Science, College of Chemical Engineering and Environmental, Liaoning Shihua University, Fushun 113001, China

[2] Thermochemistry Laboratory, Dalian Institute of Chemical Physics, Chinese Academy of Science, Dalian 116023, China

Introduction

As biological trace elements, rare earth elements and transition metal elements (such as Cu) play a certain role in the human body. Amino acids are the basic unit of the human beings. And the amino acid has two or more types of coordinated atoms and can act as various kinds of bridging ligands by using the carboxylate [1–7]. Imidazole is also involved in the important biological processes [8, 9]. As the two nitrogen atoms in one imidazole molecule are a good resource to coordinate with metal ions, some complexes based on rare earth or transition metal ions and imidazole have been reported [10–12]. Here, europium ions, copper ions, glycine, and imidazole were chosen to prepare the complex, which may have special biological properties. For the structure of Cu^{2+} ions coordinating to the nitrogen of the imidazole rings have been found presenting in the biomolecules such as histidine [13–17]. The Cu^{2+} ions bind to the imidazole rings of several histidine residues, form an important functional group in proteins, and play a key role in the mechanism of several metalloenzymes [18–20].

The synthesization, crystal structures of rare earth elements, and transition metal elements' complex were reported. The thermal stability of the complex was investigated. The basic and important thermodynamic data molar heat capacity, $C_{p,m}$, and thermodynamic properties of the complex were studied, from which many other thermodynamic properties can be calculated [21, 22].

Experimental

Synthesis of the complex

The starting materials were the analytical reagent from the Beijing Chemical Reagent Co. The solutions of Eu^{3+} and

Cu^{2+} were synthesized by dissolving excess Eu_2O_3 and CuO in a certain amount of perchloric acid (1:1). The concentrations of the above two solutions were determined by EDTA titration analysis. The glycine was added to the solutions of Eu^{3+} and Cu^{2+} for further 2 h. After the pH value of the reaction mixture was carefully adjusted to about 6.0 by the slow addition of 1.0 M NaOH solution, imidazole was added in molar ratio of $Eu^{3+}:Cu^{2+}:$-Gly:Im = 1:6:6:6. The solution was filtered to remove the precipitate after stirring for a further 4 h and placed in a desiccator filled with the silica gel. Blue crystals were generated about one month later.

An elemental analysis apparatus (Model PE-2400 II, USA) was used to measure the C, H, N of the complex. The Cl amount in ClO_4^- of the complex was determined by the ion chromatography (Waters Alliance® 2695 System with the Waters Conductivity Detector and Waters Micromass® Quattro micro™ Mass Spectrometer). The mass fraction of Eu and Cu was determined by the determination of ClO_4^- of the complex. Found: Eu (7.389 %), Cu (19.136 %), C (17.794 %), N (11.409 %), H (3.009 %) and Cl (15.665 %), which is close to the theoretical value, Eu (7.282 %), Cu (18.296 %) C (17.265 %), N (12.081 %), H (2.753 %), and Cl (15.195 %). The sample formula was determined to be $C_{30}H_{57}Cl_6Cu_6EuN_{18}O_{42}$.

X-ray structure determinations

Suitable single-crystal structure was obtained as described below by the X-ray single-diffraction study. Data collections were performed on a CCD area-detector diffractometer with graphite monochromated Mo Kα radiation ($\lambda = 0.71073$ Å at 298 K) in the ω-scan mode. Unit-cell parameters were obtained by least squares methods in the θ ranges of 2.556°–28.183° for the complex. The structures were solved by direct methods with S_{HELXS}-97 [23] and refined by full-matrix least squares methods on F^2 with S_{HELXL}-97 [24]. Anisotropic displacement parameters were refined for all non-hydrogen atoms. Hydrogen atoms were generated geometrically, assigned appropriated isotropic thermal parameters, and included in structure factor calculations. CCDC 1025592 contains the supplementary crystallographic data.

Adiabatic calorimetry and DSC analysis of the complex

Adiabatic calorimetry is the most accurate approach to achieve the heat capacity. In the present study, heat capacity measurements were taken in a high-precision automatic adiabatic calorimeter over the temperature range from 80 to 370 K. The instrument was established in Thermochemistry Laboratory of Dalian Institute of Chemical Physics,

Chinese Academy of Sciences. The structure and principle of the adiabatic calorimeter have been reported in detail elsewhere [25, 26]. A precision miniature platinum resistance thermometer (produced by Shanghai Institute of Industrial Automatic Meters, 16 mm long, 1.6 mm in diameter) measured the temperature of the sample cell. The thermometer was calibrated in terms of ITS-90 by Station of Low-Temperature Metrology and Measurements, Chinese Academy of Sciences, $R_0 = 100.1384$ Ω.

A differential scanning calorimeter (DSC-141, SETARAM, France) was utilized to perform the thermal analysis of the complexes from (300 to 700 K) at the heating rate of 10 K min^{-1} under nitrogen. The calibrations for the temperature and heat flux of the calorimeter were performed prior to the experiment. The temperature scale was calibrated by measuring the melting points of Hg, In, Sn, Pb, and Zn, at different heating rates, and the heat flux was calibrated by the Joule effect. Measurement of the melting temperature and the enthalpy of fusion of benzoic acid (NIST, Standard Reference Material 39i) were made in our laboratory to check the accuracy of the instrument.

The TG measurement of the sample was carried out by a thermogravimetric analyzer (Model: DT -20B, Shimadzu, Japan) at the heating rate of 10 K min^{-1} under a purity nitrogen with flow rate of 30 mL min^{-1}. The reference crucible was filled with α-Al_2O_3. The TG-DTG equipment was calibrated by the SRM in the thermal analysis, $CaC_2O_4 \cdot H_2O$(s).

Results and discussion

Structure of the complex

A summary of crystal data and structure refinement of the complex are provided in Table 1. The structure diagram was shown in Fig. 1. It can be seen from Fig. 1 that six Cu^{2+} ions exist around an Eu^{3+} ion in the center. Every identical two Cu^{2+} ions are connected by a chelating glycine ligand. Eu^{3+} ions have a nine-coordinated O_9 donor set (site), and its coordination polyhedron may be best described as a tricapped trigonal prism. Six apexes are formed by the six carboxylate oxygen atoms from six glycine, and three caps are formed by the three oxygen atoms from three μ_3-OH$^-$ groups. Each cation consists of three μ_3-OH$^-$ groups, which are situated in the same place with Eu^{3+} ions, forming two equilateral triangles. Glycinato ligand adopts a π-coordination mode, chelating to two Cu^{2+} and one Eu^{3+} ions. Each imidazole ligand coordinates with one Cu^{2+} ion as a terminal ligand. The two corresponding imidazole ligands in the two layers are nearly parallel. The huge network of intra- or inter-

Table 1 Crystallographic data and structure determination details for the complex

Formula	$C_{30}H_{57}Cl_6Cu_6 EuN_{18} O_{42}$
Mr	2087.84
Cryst. system	Trigonal
Space group	R3
a/Å	15.8673(12)
b/Å	15.8673(12)
c/Å	23.4038(16)
α/°	90
β/°	90
γ/°	120
Volume/Å^3	5103.0(6)
Z	3
d_{caled}/g cm^{-3}	2.038
F(000)	3972
Measured reflections	8539
Independent reflections	3704
R (int)	0.0344
Goodness of fit on F^2	1.032
Final R indices [$I > 2\sigma(I)$]	$R_1 = 0.0364$, $\omega R_2 = 0.0904$
R indices (all data)	$R_1 = 0.0400$, $\omega R_2 = 0.0929$
Largest difference peak and hole (e nm^{-3})	1.051 and -0.755
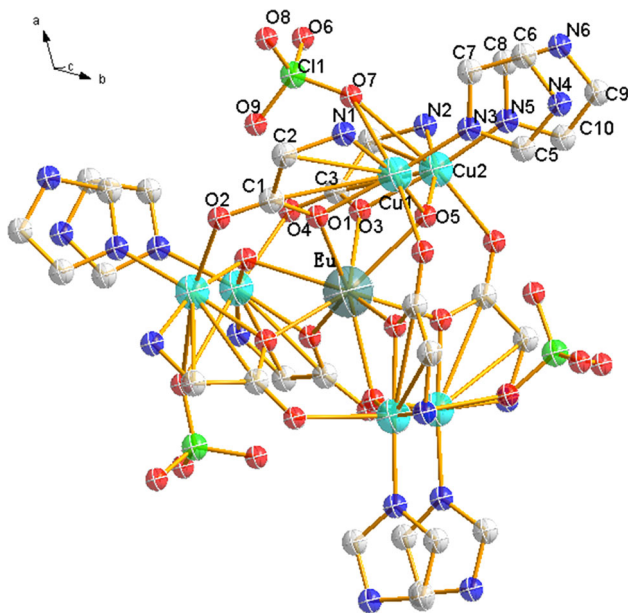
Fig. 1 Three-dimensional structure of the complex

molecular hydrogen bonds helps to stabilize the crystal. Three of the perchlorates show disorder site in the crystal, which were due to the rotation of the perchlorate groups.

Molar heat capacities and thermodynamic functions

The experimental molar heat capacities ($C_{p,m}$) of [EuCu$_6$(μ-OH)$_3$(Gly)$_6$Im$_6$](ClO$_4$)$_6$·3H$_2$O from 80 to 370 K are presented in Table 2, and the molar heat capacity values are plotted as a function of temperature in Fig. 2. The above figure shows that there is no phase change in the temperature range from 80 to 370 K.

A polynomial equation was obtained by the least square fitting by using the experimental molar heat capacities ($C_{p,m}$) and the experimental temperatures (T).

From 80 to 370 K (solid phase):

$$C_{p,m}/(\text{J K mol}^{-1}) = 917.1 + 524.2x - 89.75x^2 + 25.76x^3 + 68.52x^4 - 20.25x^5 - 35.08x^6 \quad (1)$$

where x is the reduced temperature, $x = [(T/\text{K}) - 225]/145$, T is the experimental temperature, 225 is obtained from polynomial $(T_{max} + T_{min})/2$, 145 is obtained from polynomial $(T_{max} - T_{min})/2$, T_{max} is the upper limit (370 K) of the above temperature region, T_{min} is the lower limit (80 K) of the above temperature region. Correlation coefficient R^2 of least square fitting is 0.9999.

The thermodynamic functions [$H_T - H_{298.15}$] and [$S_T - S_{298.15}$] of the compound were calculated and are listed in Table 3, which is in the temperature range from 80 to 370 K with a temperature interval of 5 K in terms of the polynomials of heat capacity and the thermodynamic relationships as Eqs. (2–5).

$$\Delta H_m = \int C_{p,m} dT \quad (2)$$

$$\Delta S_m = \int \frac{C_{p,m}}{T} dT \quad (3)$$

$$H_{T,m} - H_{298.15,m} = \int_{298.15}^{T} C_{p,m} dT \quad (4)$$

$$S_{T,m} - S_{298.15,m} = \int_{298.15}^{T} \frac{C_{p,m}}{T} dT \quad (5)$$

DSC and TG analysis

DSC analysis of the complex from the room temperature to 900 K is plotted in Fig. 3. It showed that there were two peaks in the curve. The first one was a sharp endothermic peak at 515 K, which showed the fastest rate of the decomposition. For the coexistent of the ClO$_4^-$ ions and imidazole, the rate of the decomposition was so fast. The second peak was exothermic course, which was attributed to the formation of the oxides of elements Eu and Cu.

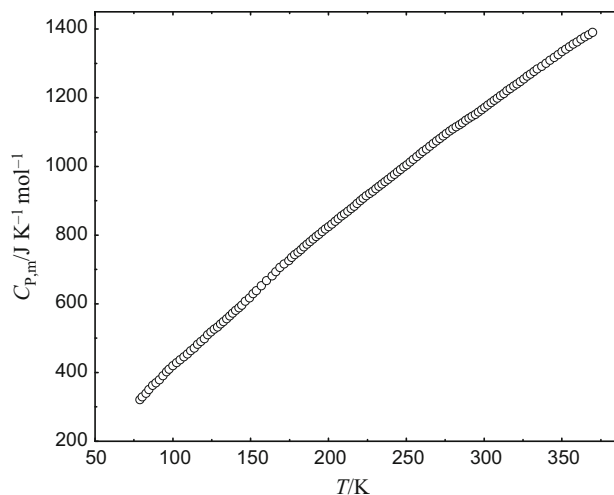**Table 2** Experimental molar heat capacities of the complex from 80 to 370 K[a]

T/K	$C_{p,m}$/J K^{-1} mol^{-1}	T/K	$C_{p,m}$/J K^{-1} mol^{-1}
80.387	328.62	149.40	616.72
82.806	339.39	151.53	629.39
84.655	350.15	153.66	638.25
87.074	362.18	156.94	652.18
89.209	369.78	160.21	667.38
91.485	378.65	163.91	681.31
93.762	390.04	166.18	693.18
95.896	402.07	168.89	705.81
97.603	409.67	171.59	715.88
100.02	419.80	174.58	725.39
102.44	428.67	176.43	734.9
104.72	436.90	178.42	743.13
107.14	445.76	180.41	749.66
109.41	454.00	182.41	757.61
111.55	463.49	184.26	765.84
113.82	471.09	186.25	773.08
115.96	481.86	188.24	780.60
118.09	490.09	190.09	787.84
120.23	498.32	192.08	795.50
122.36	509.72	193.93	801.60
124.50	517.95	196.06	809.84
126.63	526.18	198.06	817.78
128.76	532.51	200.05	824.60
130.76	541.38	202.18	831.87
132.61	547.71	204.32	840.24
134.60	555.94	206.31	847.19
136.59	564.17	208.44	855.43
138.44	572.40	210.44	861.81
140.43	580.63	212.57	869.33
142.57	588.23	214.56	877.00
144.27	595.83	216.55	883.95
146.55	607.23	218.40	891.76
220.54	899.99	292.39	1145.9
222.39	906.94	294.38	1151.3
224.38	914.47	296.38	1157.8
226.51	921.28	298.51	1164.8
228.51	927.66	300.50	1171.5
230.50	935.19	302.49	1178.7
232.49	942.00	304.63	1185.2
234.48	948.67	306.48	1192.0
236.33	955.05	308.47	1198.4
238.32	962.29	310.60	1205.5
240.46	969.41	312.74	1211.9
242.45	976.38	314.73	1219.9
244.44	983.72	316.87	1226.3
246.43	990.68	319.14	1233.7
248.43	998.34	321.28	1240.1
250.42	1004.6	323.27	1246.7

Table 2 continued

T/K	$C_{p,m}$/J K^{-1} mol^{-1}	T/K	$C_{p,m}$/J K^{-1} mol^{-1}
252.55	1012.7	325.54	1254.3
254.54	1020.5	327.68	1262.6
256.82	1028.1	329.81	1268.3
258.96	1036.4	332.09	1275.9
260.80	1043.3	334.22	1283.3
262.94	1050.5	337.07	1291.2
265.07	1058.1	339.77	1300.2
267.35	1066.6	342.33	1308.6
269.48	1073.7	345.04	1317.0
271.62	1080.7	347.60	1325.4
273.75	1088.1	350.16	1334.0
275.74	1095.2	352.58	1340.9
278.02	1102.5	355.00	1348.5
280.01	1108.9	357.42	1355.9
282.01	1115.0	359.69	1362.2
284.28	1121.4	362.40	1370.0
286.13	1126.4	364.82	1376.7
288.27	1133.8	367.38	1383.1
290.40	1140.1	369.80	1389.6

[a] Standard uncertainty for temperature $u(T) = 0.01$ K and relative standard uncertainty for the experimental molar heat capacity $u_r(C_{p,m}) = \pm 0.3$ %. $u(x) = \sqrt{\dfrac{\sum_{i=1}^{n}(x_i - \overline{x})^2}{n(n-1)}}$ where $\overline{x}$ is the mean value of a set of measurement results, n is the experimental number, x_i is a single value in a set of measurements

Fig. 2 Experimental molar heat capacities plotted against temperature of the complex from 80 to 370 K

The TG–DTG curves plotted in Fig. 4 showed that mass loss of [EuCu$_6$(μ-OH)$_3$(Gly)$_6$Im$_6$](ClO$_4$)$_6$·3H$_2$O begin at about 325 K and end at about 800 K. The whole process

Table 3 Thermodynamic functions $[H_T–H_{298.15}]$ and $[S_T–S_{298.15}]$ of the complex[a]

T/K	$C_{p,m}/$ J mol^{-1} K^{-1}	$(H_T–H_{298.15})/$ kJ mol^{-1}	$(S_T–S_{298.15})/$ J mol^{-1} K^{-1}
80	331.04	−167.82	−892.48
85	352.20	−166.11	−871.75
90	373.23	−164.29	−851.02
95	394.17	−162.37	−830.28
100	415.06	−160.34	−809.53
105	435.92	−158.21	−788.77
110	456.76	−155.98	−768.01
115	477.61	−153.64	−747.24
120	498.46	−151.19	−726.46
125	519.32	−148.65	−705.68
130	540.17	−146.00	−684.89
135	561.02	−143.24	−664.11
140	581.84	−140.38	−643.32
145	602.63	−137.42	−622.53
150	623.37	−134.35	−601.74
155	644.04	−131.19	−580.96
160	664.62	−127.91	−560.19
165	685.09	−124.54	−539.42
170	705.43	−121.06	−518.67
175	725.64	−117.48	−497.93
180	745.69	−113.80	−477.21
185	765.56	−110.02	−456.51
190	785.25	−106.15	−435.83
195	804.74	−102.17	−415.19
200	824.02	−98.100	−394.57
205	843.08	−93.932	−374.00
210	861.93	−89.669	−353.45
215	880.56	−85.313	−332.96
220	898.96	−80.864	−312.50
225	917.15	−76.323	−292.09
230	935.12	−71.693	−271.74
235	952.89	−66.972	−251.43
240	970.46	−62.164	−231.18
245	987.85	−57.268	−210.99
250	1005.1	−52.286	−190.85
255	1022.1	−47.217	−170.78
260	1039.0	−42.064	−150.76
265	1055.8	−36.827	−130.81
270	1072.5	−31.505	−110.91
275	1089.1	−26.101	−91.077
280	1105.7	−20.613	−71.301
285	1122.1	−15.043	−51.585
290	1138.6	−9.3900	−31.925
295	1155.0	−3.6551	−12.322
298.15	1165.3	0.0000	0.0000
300	1171.4	2.1619	7.2270
305	1187.7	8.0609	26.724

Table 3 continued

T/K	$C_{p,m}/$ J mol^{-1} K^{-1}	$(H_T–H_{298.15})/$ kJ mol^{-1}	$(S_T–S_{298.15})/$ J mol^{-1} K^{-1}
310	1204.1	14.042	46.169
315	1220.5	20.105	65.566
320	1236.8	26.250	84.916
325	1253.1	32.476	104.22
330	1269.3	38.784	123.48
335	1285.4	45.174	142.69
340	1301.4	51.643	161.86
345	1317.2	58.193	180.99
350	1332.7	64.821	200.06
355	1347.9	71.526	219.09
360	1362.7	78.306	238.06
365	1377.0	85.159	256.96
370	1390.6	92.083	275.80

[a] Standard uncertainty for temperature $u(T) = 0.01$ K and relative standard uncertainty for the experimental molar heat capacity $u_r(C_{p,m}) = \pm 0.3$ %. $u(x) = \sqrt{\frac{\sum_{i=1}^{n}(x_i-\overline{x})^2}{n(n-1)}}$ where $\overline{x}$ is the mean value of a set of measurement results, n is the experimental number, x_i is a single value in a set of measurements
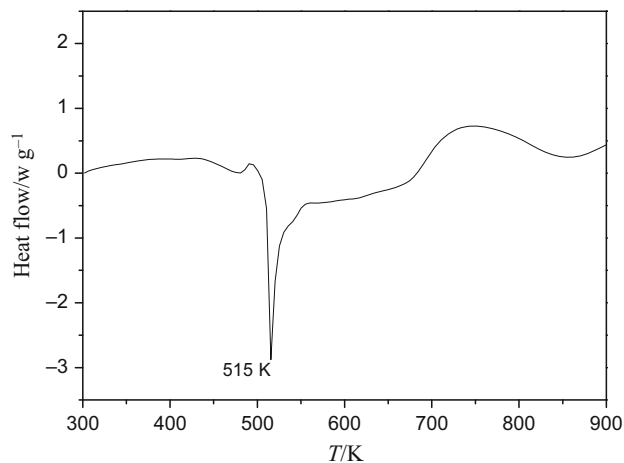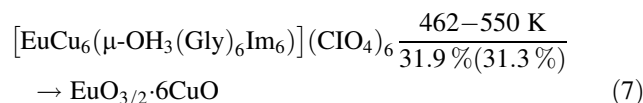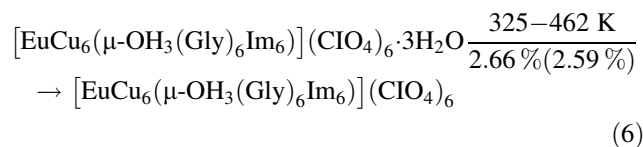

Fig. 3 DSC curve of the complex from 300 to 800 K

was divided into two stages. The mechanism was deduced as follows:

$$\left[EuCu_6(\mu\text{-}OH_3(Gly)_6Im_6)\right](ClO_4)_6 \cdot 3H_2O \xrightarrow[2.66\,\%(2.59\,\%)]{325-462\ K}$$
$$\rightarrow \left[EuCu_6(\mu\text{-}OH_3(Gly)_6Im_6)\right](ClO_4)_6$$

(6)

$$\left[EuCu_6(\mu\text{-}OH_3(Gly)_6Im_6)\right](ClO_4)_6 \xrightarrow[31.9\,\%(31.3\,\%)]{462-550\ K}$$
$$\rightarrow EuO_{3/2} \cdot 6CuO$$

(7)

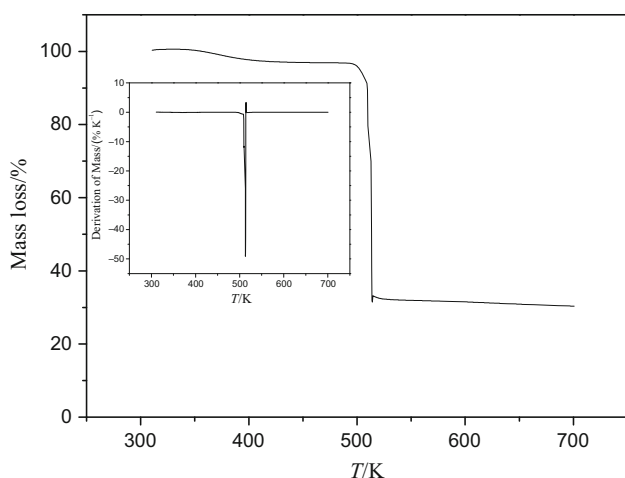**Fig. 4** TG curve of the complex from 300 to 800 K

Conclusions

In summary, $[EuCu_6(\mu\text{-OH})_3(Gly)_6Im_6](ClO_4)_6 \cdot 3H_2O$ is the rhombohedral R3 space group ($a = b = 15.8673$ Å, $c = 23.4038$ Å, $V = 5103.0(6)$ Å^3, $Z = 3$). In the cluster, Eu^{3+} ions are situated in the center of a prism formed by six copper atoms and coordinate with the nine oxygen atoms with a tricapped trigonal prismatic coordination polyhedron. Six glycinato ligands and six imidazole terminal ligands coordinated to six Cu^{2+}. The molar heat capacities of the complex were collected from 80 to 370 K, and no phase change was found in this temperature range. Moreover, the molar enthalpy and the entropy of fusion and the thermodynamic functions, $[H_T–H_{298.15}]$ and $[S_T–S_{298.15}]$, were derived from the measured heat capacity data with a temperature interval of 5 K. The DSC test found that an endothermal process happens at about 515 K, which is due to the decomposition of the ClO_4^- ions and imidazole molecules.

Supplemental data

CCDC 1025592 contains the supplementary crystallographic data for the complex.

These data can be obtained free of charge via http://www.ccdc.cam.ac.uk/ or from the Cambridge Crystallographic Data Centre, 12 Union Road, Cambridge CB2 1EZ, UK [Email: deposit@ccdc.com.ac.uk].

References

1. Yukawa Y, Inomata Y, Takeuchi T. The structure of dichloro(4-hydroxy-L-proline)cadmium(II). Bull Chem Soc Jpn. 1982;55:3135–7.
2. Inomata Y, Takeuchi T, Yukawa Y. Structure and properties of dichloro(L-proline)cadmium(II) Hydrate. Bull Chem Soc Jpn. 1983;56:2125–8.
3. Inomata Y, Yukawa Y, Yasukawa N. The structure of dichloro-bis(L-proline)zinc(II). Bull Chem Soc Jpn. 1985;58:1591–2.
4. Itoh S, Inomata Y, Yukawa Y. Structure of aquachloro(4-hydroxy-L-prolinato)copper(II). Bull Chem Soc Jpn. 1987;60:899–902.
5. Nagase M, Yukawa Y, Inomata Y, Takeuchi T. Synthetic spectroscopic and X-ray crystallographic studies of bivalent metal complexes with amino acids having a thiazolidine Ring. I. Properties of bivalent metal complexes with (S)-4-thiazolidinecarboxylic acid and the structure of chloro((S)-4-thiazolidinecarboxylato)((S)-thiazolidinium-4-carboxylate)zinc(II). Bull Chem Soc Jpn. 1988;61:775–81.
6. Inomata Y, Nakagome S, Takeuchi T. Structure and properties of chloro(N, N-diethylglycinato)copper(II). Bull Chem Soc Jpn. 1989;62:1057–60.
7. Yukawa Y. Structures and properties of (L-prolinato) copper (II) complexes prepared from different solvents. J Chem Soc Dalton Trans. 1992;22:3217–21.
8. Allen FH. The Cambridge structural database: a quarter of a million crystal structures and rising. Acta Crystallogr Sect B. 2002;58:380–8.
9. Mura P, Casini A, Marcon G, Messori L. Synthesis, molecular structure and solution chemistry of the iridium(III) complex imidazolium [trans(bisimidazole)tetrachloro iridate(III)] (IRIM). Inorg Chim Acta. 2001;312:74–80.
10. Masciocchi N, Ardizzoia GA, Brenna S, Castelli F, Galli S, Maspero A, Sironi A. Synthesis and ab initio XRPD structure of group 12 imidazolato polymers. Chem Commun. 2003;16:2018–9.
11. Lambert F, Renault JP, Policar C, Badarau IM, Cesario M. A polymeric, layered bimetallic Mn(II)Fe(III) imidazolate network; crystal structure and magnetic properties. Chem Commun. 2000;1:35–6.
12. Huang XC, Zhang JP, Lin YY, Yu XL, Chen XM. Two mixed-valence copper(I, II) imidazolate coordination polymers: metal-valence tuning approach for new topological structures. Chem Commun. 2004;9:1100–1.
13. Choi YA, Keem JO, Kim CY, Yoon HR, Heo WD, Chung BH, Jung YW. A novel copper-chelating strategy for fluorescent proteins to image dynamic copper fluctuations on live cell surfaces. Chem Sci. 2015;6:1301–6.
14. Dede B, Karipcin F, Cengiz M. Novel homo-and hetero-nuclear copper (II) complexes of tetradentate Schiff bases: synthesis, characterization, solvent extraction and catalase—like activity studies. J Hazard Mater. 2009;163:1148–56.
15. William MA, Sarah CL. DFT calculations of the EPR parameters for Cu(II) DETA imidazole complexes. Phys Chem Chem Phys. 2009;11:8266–74.
16. Lakatos A, B′ela G, N′ora VN, Zita C, W′eber E, L′ıvia F, Tam′as K. Histidine-rich branched peptides as Cu(II) and Zn(II) chelators with potential therapeutic application in Alzheimer's disease. Dalton Trans. 2012;41:1713–26.
17. Remelli M, Valensin D, Bacco D, Gralka E, Guerrini R, Migliorini C, Kozlowskic H. The complex-formation behaviour of His residues in the fifth Cu^{2+} binding site of human prion protein: a close look. New J Chem. 2009;33:2300–10.

18. Jorge AT, Luis RS, Mariona S. Computational calculations of pK_a values of imidazole in Cu(II) complexes of biological relevance. Phys Chem Chem Phys. 2011;13:7852–61.

19. Potocki S, Valensinb D, Kozlowski H. The specificity of interaction of Zn^{2+}, Ni^{2+} and Cu^{2+} ions with the histidine-rich domain of theTjZNT1 ZIP family transporter. Dalton Trans. 2014;43:10215–23.

20. Gralka E, Valensin D, Porciatti E, Gajda C, Gaggelli E, Valensin G, Kamysz W, Nadolny R, Guerrini R, Bacco D, Remelli M, Kozlowski H. Cu^{II} binding sites located at His-96 and His-111 of the human prion protein: thermodynamic and spectroscopic studies on model peptides. Dalton Trans. 2008; 38:5207–19.

21. Novikov VV, Avdashchenko DV, Matovnikov AV, Mitroshenkov NV, Bud'ko SL. Heat capacity and thermal expansion of icosahedral lutetium boride LuB_{66}. J Thermal Anal Calorim. 2014;116:765–9.

22. Galkin V, Gartvich Y. Thermal expansion and evaluation of almandine heat capacity. J Therm Anal Calorim. 2015;1–6. doi:10.1007/s10973-015-4768-9.

23. Sheldrick GM. A short history of SHELX. Acta Crystallogr Sect A. 2008;64:112–22.

24. Weng NS. Some strategies for the refinement of disordered structures with the SHELXL-97 refinement program. Chin J Struct Chem. 2005;24:1425–39.

25. Zhong WW, Di YY, Dou JM. Synthesis, structural characterization, and thermochemistry of complexes of pyridine 2,6-dicarboxylate with metals (Mg and Sr). J Thermal Anal Calorim. 2014;115:2527–33.

26. Wang Z, Li B, Zhang YH, Wang M, Kong YX, Di YY, Dou JM. Molar heat capacities and solution thermochemistry of n-undecylammonium bromide monohydrate $C_{11}H_{28}BrNO(s)$. J Thermal Anal Calorim. 2015;120:1645–55.